

Einstein-Podolsky-Rosen correlations in spontaneous parametric down-conversion: Beyond the Gaussian approximation

A. G. da Costa Moura^{1,*} and C. H. Monken^{2,†}

¹*Instituto de Ciência e Tecnologia, Universidade Federal dos Vales do Jequitinhonha e Mucuri, Rodovia MGT 367 - km 583, N 5000, Alto da Jacuba, Diamantina, MG 39100-000, Brazil*

²*Departamento de Física, ICEx, Universidade Federal de Minas Gerais, Av. Antonio Carlos, 6627, Belo Horizonte, MG, 31270-901, Brazil*

(Dated: May 21, 2024)

We present analytic expressions for the coincidence detection probability amplitudes of photon pairs generated by spontaneous parametric down-conversion in both momentum and position spaces, without using the Gaussian approximation and taking into account the effects of birefringence in the nonlinear crystal. We also present experimental data supporting our theoretical predictions, using Einstein-Podolsky-Rosen correlations as benchmarks, for 8 different pump beam configurations.

I. INTRODUCTION

Spontaneous parametric down-conversion (SPDC) is a versatile and widely used tool in investigating fundamental quantum properties of correlated two-photon fields. Among these properties, nonclassical transverse momentum and transverse position correlations in two-photon states have been explored in many works with SPDC, in particular, the so-called Einstein-Podolsky-Rosen (EPR) paradox [1], first realized experimentally by Howell *et al.* [2] and by D'Angelo *et al.* [3].

Realizing the EPR paradox consists of preparing a quantum state of two spatially separated particles that allows one to infer with high precision either the position or the momentum of one of the particles (say, particle 1) without interacting with it, by measuring the position or the momentum of the other particle (particle 2). Since the measurement of x_2 or p_2 is a matter of choice, and x and p are incompatible variables and therefore subjected to the uncertainty relation $\Delta x \Delta p \geq \hbar/2$, EPR used the possibility to prepare such a state and the hypothesis of locality to suggest that Quantum Mechanics is an incomplete theory although it is correct in its statistical predictions. After a long debate, remarkable theoretical developments, and a long series of experiments [4], the idea that local hidden-variable theories are ruled out is now common sense. Nevertheless, EPR-type correlations are interesting on their own [5] and have been studied over the last two decades in two-photon states generated by SPDC [6–18].

As a rule, most works on EPR-type correlations in SPDC either rely on oversimplified models to describe the two-photon quantum state or do not present a theoretical model in both momentum and position representations to fit experimental data. In general, those simplified models do not include the effects of birefringence in the nonlinear crystals used in practice. Because of this, EPR correlations in SPDC have been analyzed only in

the direction that is not affected by birefringence, that is, the direction normal to the plane defined by the crystallographic optic axis and the pump beam propagation direction [19]. The commonly used Gaussian models to describe SPDC two-photon states have the advantage of simplifying calculations, but fail to correctly describe the full state propagation and do not include the effects of birefringence. A detailed discussion of Gaussian approximations in SPDC can be found in ref. [20], although in comparison with a simplified non-Gaussian model.

Experimental conditions such as the pump laser beam focusing, the nonlinear crystal length, and birefringence can affect EPR correlations in a way that is not explained by previous models. In this work, we present a more precise theoretical model for the SPDC two-photon state in both position and momentum representations and show how well it fits experimental data.

This paper is organized as follows. In Sec. II we explain the meaning of the Gaussian approximation in SPDC and present an accurate expression for the two-photon state generated by SPDC in both momentum and position representations without making use of that approximation. In Sec. III we describe EPR correlations in the two-photon states generated by SPDC and how they depend on experimental conditions. In Sec. IV we present an experiment where we measured EPR correlations in SPDC with eight different pump beam configurations, to validate our theoretical predictions. In Sec. V we present a brief discussion of the results and our conclusions.

II. THE TWO-PHOTON STATE GENERATED BY SPDC

The basic SPDC process occurs when one photon from the laser pump beam of frequency ω_p , usually in the ultra-violet spectral range, is converted into two photons of frequencies ω_1 and ω_2 , such that $\omega_1 + \omega_2 = \omega_p$ (energy conservation) and $\mathbf{k}_1 + \mathbf{k}_2 \approx \mathbf{k}_p$ (phase match). Due to dispersion, the refractive index at ω_p is greater than it is at the lower frequencies ω_1 and ω_2 , making phase match

* alex.gutenberg@ict.ufvjm.edu.br

† monken@fisica.ufmg.br

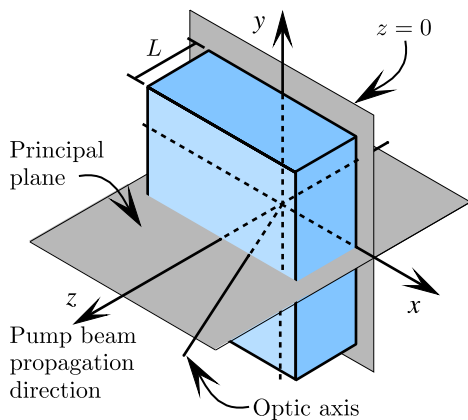


FIG. 1. Nonlinear crystal configuration.

impossible in isotropic media. This problem is circumvented in birefringent nonlinear media, where dispersion can be compensated by birefringence. For example, in negative uniaxial crystals [21], such as BBO, the pump beam polarized in the extraordinary direction and the down-converted beams polarized in the ordinary direction can be subjected to the same refractive indices, provided they propagate at appropriate directions. If the pump laser beam with extraordinary polarization propagates at an angle θ with respect to the optic axis direction inside the crystal, it is subjected to a refractive index [19]

$$\eta_p = \frac{n_{op}n_{ep}}{n_{op}^2 \sin^2 \theta + n_{ep}^2 \cos^2 \theta}, \quad (1)$$

where n_{op} and n_{ep} are the ordinary and extraordinary refractive indices, respectively, at ω_p . The collinear type I phase match condition is achieved when θ is such that, $\eta_p \omega_p = n_{o1} \omega_1 + n_{o2} \omega_2$, where n_{o1} and n_{o2} are the ordinary refractive indices at frequencies ω_1 and ω_2 , respectively.

Let us consider a piece of negative birefringent nonlinear crystal (e.g., BBO) in the form of a block having its input face lying on the plane $z = 0$, and cut for type I phase match with the principal plane (defined by optic axis and the pump beam propagation axis) parallel to the plane xz . A uv pump beam whose cross section lies entirely within the input and output faces of the crystal propagates along the z axis with extraordinary (x) polarization. The crystal thickness in the z direction is L . This configuration is illustrated in Fig. 1.

In the \mathbf{k} -vector (momentum) representation, the two-photon detection probability amplitude for the state generated by SPDC in the paraxial approximation is known to be well described (up to a normalization constant) by [22]

$$\psi(\mathbf{q}_1, \mathbf{q}_2) = \mathcal{E}_0(\mathbf{q}_1 + \mathbf{q}_2) e^{-i\Delta_{oo}} \text{sinc } \Delta_{oo}, \quad (2)$$

where \mathbf{q}_j is the xy component of \mathbf{k}_j ($j = 1, 2$), $\mathcal{E}_0(\mathbf{q})$ is the angular spectrum of the pump beam on the plane

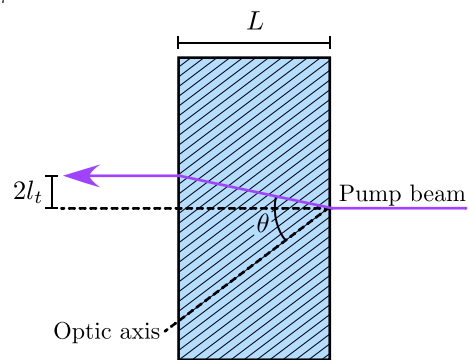


FIG. 2. The walk-off of the pump beam in a negative uniaxial crystal.

$z = 0$,

$$\Delta_{oo} = \mu_{oo} + l_t(q_{1x} + q_{2x}) - \frac{L}{4k_p} \left| \sqrt{\frac{\omega_2}{\omega_1}} \mathbf{q}_1 - \sqrt{\frac{\omega_1}{\omega_2}} \mathbf{q}_2 \right|^2,$$

$k_p = \eta_p \omega_p / c$, l_t is half of the transverse walk-off length, $\mu_{oo} = (\bar{n}_o - \eta_p) k_p L / 2 \eta_p$, and \bar{n}_o is the ordinary refractive index of the nonlinear crystal at $\omega_p / 2$. The transverse walk-off length is given by [19]

$$2l_t = \frac{(n_{op}^2 - n_{ep}^2) \sin \theta \cos \theta}{n_{op}^2 \sin^2 \theta + n_{ep}^2 \cos^2 \theta} L. \quad (3)$$

In negative uniaxial crystals, $n_{ep} < n_{op}$ and the extraordinary beam tends to deviate away from the optic axis direction. This situation is illustrated in Fig. 2

Here we work in the collinear phase match condition, where $\bar{n}_o = \eta_p \rightarrow \mu_{oo} = 0$, and in the quasi-degenerate regime, where $\omega_1 = (1 + \nu) \omega_p / 2$ and $\omega_2 = (1 - \nu) \omega_p / 2$, with $\nu \ll 1$. This means that $\sqrt{\omega_2 / \omega_1} \approx 1 - \nu$ and $\sqrt{\omega_1 / \omega_2} \approx 1 + \nu$. In the collinear phase match it is possible to make a straightforward use of the paraxial approximation and Fourier optics [23]. It is also possible to do so in the noncollinear phase match but at the cost of more complicated expressions. We chose to work in the quasi-degenerate regime in order to stress the generality of our model. The degenerate regime can be readily recovered by making $\nu = 0$ in the expressions that follow. It is interesting to notice that even in the collinear regime there will be a walk-off in the propagation of the pump beam inside the nonlinear crystal, since the phase match angle θ lies, in general, between 0 and $\pi/2$. In our experiment (see section IV), $\theta \approx 33^\circ$.

To simplify the notation, we make

$$\begin{aligned} \mathbf{Q} &= \mathbf{q}_1 + \mathbf{q}_2, \\ \mathbf{P} &= (1 - \nu) \mathbf{q}_1 - (1 + \nu) \mathbf{q}_2, \\ \beta^2 &= \frac{L}{4k_p}. \end{aligned} \quad (4)$$

Then,

$$\psi(\mathbf{Q}, \mathbf{P}) = \mathcal{E}_0(\mathbf{Q}) \text{sinc}(l_t Q_x - \beta^2 P^2) e^{-i(l_t Q_x - \beta^2 P^2)}. \quad (5)$$

Since $\psi(\mathbf{Q}, \mathbf{P})$ is a two-beam plane-wave spectrum and the two beams propagate independently by acquiring a phase factor depending on the z -component of each \mathbf{k} -vector [23], on the output face of the nonlinear crystal, at $z = L$, the propagated $\psi(\mathbf{Q}, \mathbf{P})$ is

$$\psi(\mathbf{Q}, \mathbf{P}, L) = \psi(\mathbf{Q}, \mathbf{P}) e^{i(k_{1z} + k_{2z})L}. \quad (6)$$

Inside the crystal, in the collinear phase match [22],

$$\begin{aligned} (k_{1z} + k_{2z})L &= \frac{\bar{n}_o L}{c} (\omega_1 + \omega_2) \\ &- \frac{Lc}{\bar{n}_o} [(1 - \nu)q_1^2 + (1 + \nu)q_2^2] \\ &= k_p L - 2\beta^2(Q^2 + P^2). \end{aligned} \quad (7)$$

Therefore,

$$\begin{aligned} \psi(\mathbf{Q}, \mathbf{P}, L) &= \mathcal{E}_0(\mathbf{Q}) \text{sinc}(l_t Q_x - \beta^2 P^2) \\ &\times e^{-i(l_t Q_x + 2\beta^2 Q^2)} e^{-i\beta^2 P^2}. \end{aligned} \quad (8)$$

Considering a Gaussian pump beam, we can write, in the complex notation [24],

$$\mathcal{E}(\mathbf{Q}, z) = A e^{ik_p^v z} e^{-ia(z)Q^2/2k_p^v}, \quad (9)$$

where A is a constant, $k_p^v = \omega_p/c$ (superscript v stands for vacuum), $a(z) = z - z_c - ik_p^v w_0^2/2$, w_0 is the beam waist and z_c is the waist location on the z axis. Hence,

$$\mathcal{E}_0(\mathbf{Q}) = A e^{-ia_0 Q^2/2k_p^v}, \quad (10)$$

where $a_0 = a(0)$. Then, at the output face of the crystal,

$$\begin{aligned} \psi(\mathbf{Q}, \mathbf{P}, L) &= e^{-i(a_0/2k_p^v + 2\beta^2)Q^2} e^{-il_t Q_x} e^{-i\beta^2 P^2} \\ &\times \text{sinc}(l_t Q_x - \beta^2 P^2). \end{aligned} \quad (11)$$

From $z = L$ to $z > L$, $\psi(\mathbf{Q}, \mathbf{P})$ propagates in free space, that is,

$$\psi(\mathbf{Q}, \mathbf{P}, z) = \psi(\mathbf{Q}, \mathbf{P}, L) e^{i(k_{1z}^v + k_{2z}^v)(z-L)}. \quad (12)$$

In free space and collinear propagation,

$$\begin{aligned} (k_{1z}^v + k_{2z}^v)(z - L) &= \left(k_1^v + k_2^v - \frac{q_1^2}{2k_1^v} - \frac{q_2^2}{2k_2^v} \right) (z - L) \\ &= k_p^v (z - L) + 2\bar{n}_o \beta^2 (Q^2 + P^2) \\ &- \frac{z}{2k_p^v} (Q^2 + P^2). \end{aligned} \quad (13)$$

Therefore,

$$\begin{aligned} \psi(\mathbf{Q}, \mathbf{P}, z) &= \text{sinc}(l_t Q_x - \beta^2 P^2) e^{-il_t Q_x} \\ &\times e^{-ib_1(z)Q^2} e^{-ib_2(z)P^2}, \end{aligned} \quad (14)$$

where

$$\begin{aligned} b_1(z) &= a(z)/2k_p^v - 2(\bar{n}_o - 1)\beta^2, \\ b_2(z) &= z/2k_p^v - (2\bar{n}_o - 1)\beta^2. \end{aligned} \quad (15)$$

To the best of our knowledge, an accurate analytic expression for ψ in the coordinate representation is not available in the literature, except under the Gaussian approximation, which consists of replacing $\text{sinc}(l_t Q_x - \beta^2 P^2)$ in Eq. (14) by a Gaussian function, necessarily neglecting the walk-off term $l_t Q_x$. This approximation works well when $L/k_p w_0^2 \ll 1$, that is, when the pump beam is highly collimated, or when the crystal is very thin ($L \approx 1$ mm) [20].

To arrive at an expression for ψ , in coordinate representation, we adopt the following approximation: For pump beams with reasonably narrow-band angular spectra ($w_0 \geq 50 \mu\text{m}$) and $L \sim 1$ mm to 5 mm, which cover most practical cases, we can make

$$\begin{aligned} \psi(\mathbf{Q}, \mathbf{P}, z) &= \text{sinc}(l_t Q_x) e^{-il_t Q_x} e^{-ib_1(z)Q^2} \\ &\times \text{sinc}(\beta^2 P^2) e^{-ib_2(z)P^2}, \end{aligned} \quad (16)$$

which turns $\psi(\mathbf{Q}, \mathbf{P}, z)$ into a separable function of \mathbf{Q} and \mathbf{P} .

Defining the coordinates $\mathbf{R} = [(1 + \nu)\boldsymbol{\rho}_1 + (1 - \nu)\boldsymbol{\rho}_2]/2$ and $\mathbf{S} = (\boldsymbol{\rho}_1 - \boldsymbol{\rho}_2)/2$, the calculation of the Fourier transform of $\psi(\mathbf{Q}, \mathbf{P}, z)$ is straightforward:

$$\begin{aligned} \psi(\mathbf{R}, \mathbf{S}, z) &= \frac{e^{-R_y^2/4ib_1(z)}}{l_t \sqrt{ib_1(z)}} \\ &\times \left\{ \text{Erf} \left[\frac{R_x - 2l_t}{2\sqrt{ib_1(z)}} \right] - \text{Erf} \left[\frac{R_x}{2\sqrt{ib_1(z)}} \right] \right\} \\ &\times \left\{ \text{Ei} \left[\frac{ik_p^v S^2}{2(z - L)} \right] - \text{Ei} \left[\frac{ik_p^v S^2}{2(z - L')} \right] \right\} \end{aligned} \quad (17)$$

for $z > L$, where $L' = (1 - 1/\bar{n}_o)L$, Erf is the error function, and Ei is the exponential integral function [25].

Eqs. (16) and (17) can be considered the main contribution of this work to the field of SPDC. Using Eq. (17) one can predict experimental results of spatial two-photon correlations with very good accuracy and push experimental conditions to their limits when testing specific theoretical models. In this work, we test EPR correlations, as they involve both spatial and momentum correlations.

III. EPR CORRELATIONS

With expressions (16) and (17) we can calculate the uncertainties Δx_1 , Δy_1 , for fixed x_2 , y_2 and z , and Δk_{x1} , Δk_{y1} for fixed k_{x2} , k_{y2} as functions of the pump beam angular spectrum width (defined by the beam waist w_0) and see how they are affected by the crystal anisotropy (quantified here by walk-off parameter l_t). Assuming any fixed value for $\boldsymbol{\rho}_2$, Eq. (17) allows us to calculate Δx_1

TABLE I. Pump beam parameters.

Beam	w_0 (mm)	z_c (mm)
1	0.062	178
2	0.067	213
3	0.072	251
4	0.085	298
5	0.095	355
6	0.105	422
7	0.120	510
8	0.142	635

and Δy_1 for any $z > L$. Alternatively, assuming any fixed value for \mathbf{q}_2 , Eq. (16) allows us to calculate Δk_{1x} and Δk_{1y} , which do not depend on z . As an example, Fig. 3 shows plots of Δx_1 and Δy_1 for $\rho_2 = 0$ and plots of Δk_{x1} and Δk_{y1} for $\mathbf{q}_2 = 0$, for a 5 mm-long BBO crystal pumped by 355 nm gaussian laser beams whose waists w_0 and waist positions z_c are shown in Table I. Uncertainties Δx_1 and Δy_1 were calculated on the plane $z = 5.0001$ mm.

One can see that while the position uncertainties in the x and y directions are about the same, the momentum uncertainties are strongly affected by the anisotropy. This is a direct consequence of the partial transfer of the pump beam angular spectrum in the direction parallel to the principal plane [19], in our case, the x direction.

It is interesting to note that the uncertainties Δx_1 and Δy_1 increase rapidly as the distance from the crystal increases in the z direction. In general, position uncertainties depend on the pump beam parameters, as exemplified in Fig. 4. For a weakly focused laser beam ($w_0 = 0.5$ mm) whose waist is located at the crystal input face ($z = 0$), our predictions shown in Fig. 4a are in good agreement with the results reported in Ref [17]. This agreement is because in this case a Gaussian model fits well the uncertainty in position coordinates [20].

IV. EXPERIMENT

EPR correlations predicted in the previous section were tested experimentally with the setup represented in Fig. 5. A 5 mm-long BBO crystal cut for type I collinear phase match (*NLC*) having its optic axis parallel to the xz plane and input face located on the plane $z = 0$ was pumped by a 355 nm laser beam polarized in the x direction, propagating along the z direction. The beam parameters, listed in Table I, were changed with the help of a telescope composed by a lens L_3 of focal length 50 mm and a lens L_4 of focal length 40 mm separated from L_3 by a variable distance. The down-converted light, with $\lambda_1 = 690$ nm and $\lambda_2 = 731$ nm was sent to a beam splitter (*BS*) and directed to detectors D_1 (equipped with a 12 nm band-pass filter centered at 690 nm) and D_2 (equipped with a 40 nm band-pass filter centered at 730 nm). Lenses L_1 and L_2 of focal length

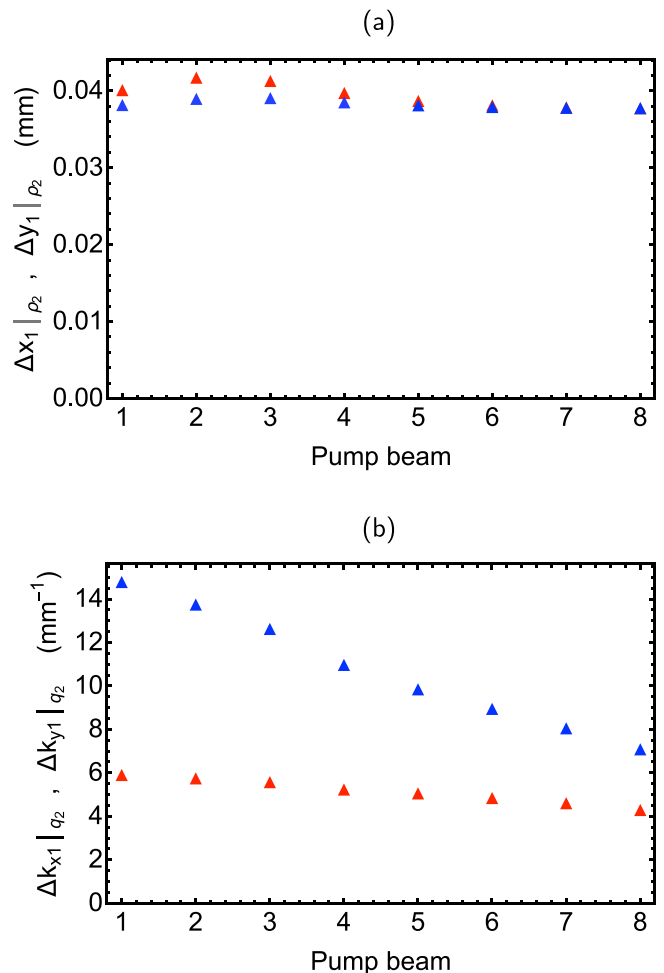


FIG. 3. Predicted values of (a) $\Delta x_1|_{\rho_2=0}$ (red) and $\Delta y_1|_{\rho_2=0}$ (blue), (b) $\Delta k_{x1}|_{q_2=0}$ (red) and $\Delta k_{y1}|_{q_2=0}$ (blue) for a 5 mm-long BBO crystal pumped by 355 nm laser beams whose parameters are listed in Table I.

75 mm were placed at 150 mm from the output face of the nonlinear crystal. Detectors D_1 and D_2 were placed at 75 mm from L_1 and L_2 (Fourier plane) for the measurements of $|\psi(\mathbf{q}_1, 0, L)|^2$ and at 150 mm (1:1 image plane) for the measurements of $|\psi(\boldsymbol{\rho}_1, 0, L)|^2$. Each detector consists of a multimode optical fiber with a diameter of 50 μm , one tip mounted on a computer-controlled xy motorized translation stage and the other tip coupled to a photon-counting avalanche photodiode. In all measurements, D_2 was kept at $\rho_2 = 0$.

Due to the relatively large fiber diameter and photon-counting fluctuations, experimental results are not directly comparable with theory. To check the accuracy of theoretical predictions, the following procedure was adopted: Experimental data for coincidence detections on the image plane were fit to a hyperbolic secant distribution $A \text{sech} \pi\xi/2\Delta_\xi$ ($\xi = x, y$), whose standard deviation is given by Δ_ξ . Numerical convolutions of the theoretical coincidence profiles with the 50 μm circular

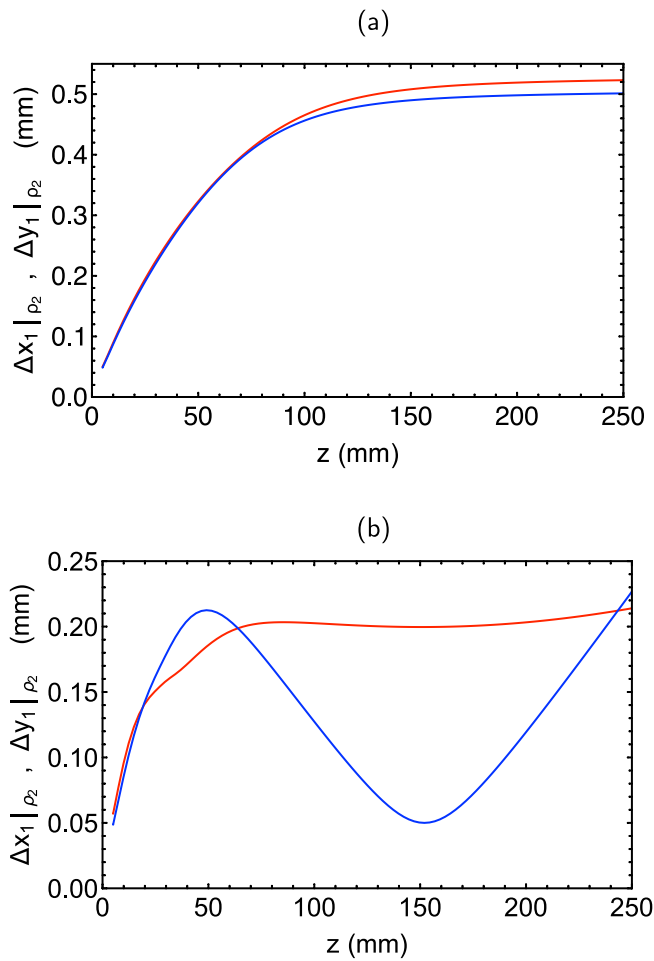


FIG. 4. Predicted values of $\Delta x_1|_{\rho_2=0}$ (red) and $\Delta y_1|_{\rho_2=0}$ (blue) as functions of the distance from the output face of a 5 mm-long BBO crystal cut for collinear degenerate phase match, pumped by a 355 nm laser beam with (a) $w_0 = 0.5$ mm, $z_c = 0$ and (b) $w_0 = 0.05$ mm, $z_c = 150$ mm.

apertures of D_1 and D_2 were made, resulting in the expected detection probability distributions. Profiles obtained when the crystal was pumped with the laser beam #1 (see Table I) are shown in Fig. 6. An additional correction of the beam waist radius was made, due to the pump beam M^2 factor of 1.14. On the Fourier plane, a Gaussian distribution $A \exp(-\xi^2/2\Delta_\xi^2)$ ($\xi = k_x, k_y$) was used in a similar procedure. Experimental results and theoretical predictions are presented in Fig. 7.

V. DISCUSSION AND CONCLUSION

From the results presented here, one can see that the EPR correlations $\Delta x \Delta k_x$ and $\Delta y \Delta k_y$ of the photons pairs generated by spontaneous parametric down-conversion are strongly affected by the pump beam angular spectrum in the direction normal to the principal

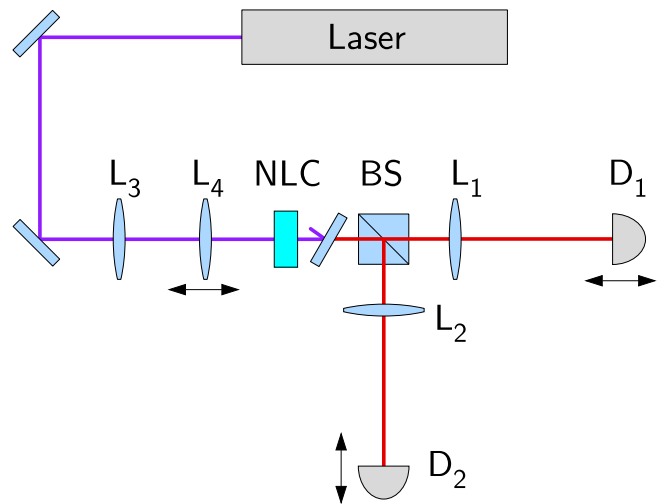


FIG. 5. Experimental setup

plane (defined by the optic axis and the z axis). Such dependence is much smaller in the direction parallel to the principal plane. This effect is readily explained by the presence of the term $\text{sinc } l_t Q_x$ in Eq. (16). That term, which depends on the birefringence, the phase match angle, and the crystal length (see Eq. (3)), acts as a spatial filter for the transfer of the angular spectrum from the pump beam to the two-photon state [19]. Because of this filtering effect, the product $\Delta x \Delta k_x$ behaves like the laser beam was less focused. The two uncertainty products $\Delta x \Delta k_x$ and $\Delta y \Delta k_y$ tend to a unique minimum value as the pump beam gets more collimated, that is, $w_0 \gg l_t$. In our case, $l_t = 0.186$ mm.

In conclusion, we have presented, unlike any previous publication: (a) Accurate analytic expressions for the coincidence detection probability amplitudes of photon pairs generated by spontaneous parametric down-conversion in both momentum and position spaces on the entire plane normal to the pump beam. Those expressions allow us to predict how the correlations in position and momentum depend on the system parameters like crystal length, crystal birefringence, pump beam focusing, pump beam waist location, and detectors locations. (b) Experimental data supporting our theoretical predictions, using Einstein-Podolsky-Rosen correlations as benchmarks, for 8 different pump beam configurations.

The results presented here may be useful in any application relying on position and momentum correlations of photon pairs generated by SPDC in birefringent crystals.

ACKNOWLEDGMENTS

This work was supported by CNPq Project 302872/2019-1 and INCT-IQ Project 465469/2014-0.

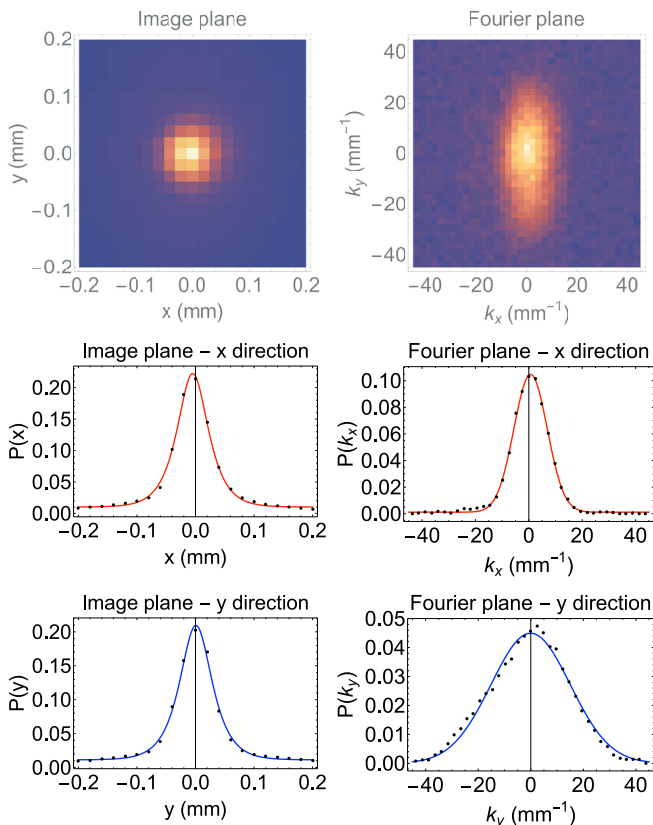


FIG. 6. Top row: Examples of coincidence detection profiles on the image plane (left) and on the Fourier plane (right) for beam # 1 (see Table I). Mid row: Corresponding detection probability densities $P(x_1|\rho_2 = 0)$ (left) and $P(y_1|\rho_2 = 0)$ (right). Bottom row: Corresponding detection probability densities $P(k_{x1}|\mathbf{q}_2 = 0)$ (left) and $P(k_{y1}|\mathbf{q}_2 = 0)$ (right). Dots are normalized experimental data and solid lines are best fits for distributions $A \operatorname{sech} \pi \xi / 2 \Delta_\xi$ ($\xi = x, y$ on the image plane) and $A \exp(-\xi^2 / 2 \Delta_\xi^2)$ ($\xi = k_x, k_y$ on the Fourier plane).

-
- [1] A. Einstein, B. Podolsky, and N. Rosen, Can quantum-mechanical description of physical reality be considered complete?, *Phys. Rev.* **47**, 777 (1935).
- [2] J. C. Howell, R. S. Bennink, S. J. Bentley, and R. W. Boyd, Realization of the Einstein-Podolsky-Rosen paradox using momentum- and position-entangled photons from spontaneous parametric down conversion, *Phys. Rev. Lett.* **92**, 210403 (2004).
- [3] M. D'Angelo, Y.-H. Kim, S. P. Kulik, and Y. Shih, Identifying entanglement using quantum ghost interference and imaging, *Phys. Rev. Lett.* **92**, 233601 (2004).
- [4] M. Genovese, Research on hidden variable theories: A review of recent progresses, *Phys. Rep.* **413**, 319 (2005).
- [5] M. D. Reid, P. D. Drummond, W. P. Bowen, E. G. Cavalcanti, P. K. Lam, H. A. Bachor, U. L. Andersen, and G. Leuchs, The Einstein-Podolsky-Rosen paradox: From concepts to applications, *Rev. Mod. Phys.* **81**, 1727 (2009).
- [6] D. S. Tasca, S. P. Walborn, P. H. S. Ribeiro, F. Toscano, and P. Pellat-Finet, Propagation of transverse intensity correlations of a two-photon state, *Phys. Rev. A* **79**, 033801 (2009).
- [7] S. P. Walborn, A. Salles, R. M. Gomes, F. Toscano, and P. H. Souto Ribeiro, Revealing hidden Einstein-Podolsky-Rosen nonlocality, *Phys. Rev. Lett.* **106**, 130402 (2011).
- [8] M. Edgar, D. Tasca, F. Izdebski, R. Warburton, J. Leach, M. Agnew, G. Buller, R. Boyd, and M. Padgett, Imaging high-dimensional spatial entanglement with a camera, *Nat. Commun.* **3**, 984 (2012).
- [9] P.-A. Moreau, J. Mougins-Sisini, F. Devaux, and E. Lantz, Realization of the purely spatial Einstein-Podolsky-Rosen paradox in full-field images of spontaneous parametric down-conversion, *Phys. Rev. A* **86**, 010101(R) (2012).

- [10] P.-A. Moreau, F. Devaux, and E. Lantz, Einstein-Podolsky-Rosen paradox in twin images, *Phys. Rev. Lett.* **113**, 160401 (2014).
- [11] J. Schneeloch and G. A. Howland, Quantifying high-dimensional entanglement with Einstein-Podolsky-Rosen correlations, *Phys. Rev. A* **97**, 042338 (2018).
- [12] E. Giese, R. Fickler, W. Zhang, L. Chen, and R. W. Boyd, Influence of pump coherence on the quantum properties of spontaneous parametric down-conversion, *Phys. Scr.* **93**, 084001 (2018).
- [13] L. Chen, T. Ma, X. Qiu, D. Zhang, W. Zhang, and R. W. Boyd, Realization of the Einstein-Podolsky-Rosen paradox using radial position and radial momentum variables, *Phys. Rev. Lett.* **123**, 060403 (2019).
- [14] B. Ndagano, H. Defienne, A. Lyons, I. Starshynov, F. Villa, S. Tisa, and D. Faccio, Imaging and certifying high-dimensional entanglement with a single-photon avalanche diode camera, *npj Quantum Inf* **6**, 94 (2020).
- [15] V. Srivastav, N. H. Valencia, S. Leedumrongwatthanakun, W. McCutcheon, and M. Malik, Characterizing and tailoring spatial correlations in multimode parametric down-conversion, *Phys. Rev. Appl.* **18**, 054006 (2022).
- [16] A. Bhattacharjee, N. Meher, and A. K. Jha, Measurement of two-photon position-momentum Einstein-Podolsky-Rosen correlations through single-photon intensity measurements, *New J. Phys.* **24**, 053033 (2022).
- [17] A. Bhattacharjee, M. K. Joshi, S. Karan, J. Leach, and A. K. Jha, Propagation-induced revival of entanglement in the angle-oam bases, *Sci. Adv.* **8**, eabn7876 (2022).
- [18] S. Patil, S. Prabhakar, A. Biswas, A. Kumar, and R. P. Singh, Anisotropic spatial entanglement, *Phys. Lett. A* **457**, 128583 (2023).
- [19] A. G. da Costa Moura, W. A. T. Nogueira, and C. H. Monken, Fourth-order image formation by spontaneous parametric down-conversion: The effect of anisotropy, *Opt. Commun.* **283**, 2866 (2010).
- [20] E. S. Gómez, W. A. T. Nogueira, C. H. Monken, and G. Lima, Quantifying the non-gaussianity of the state of spatially correlated down-converted photons, *Opt. Express* **20**, 3753 (2012).
- [21] A. Yariv and P. Yeh, *Optical Waves in Crystals: Propagation and Control of Laser Radiation* (Wiley, 2002).
- [22] S. P. Walborn, C. H. Monken, S. Pádua, and P. H. Souto Ribeiro, Spatial correlations in parametric down-conversion, *Phys. Rep.* **495**, 87 (2010).
- [23] J. W. Goodman, *Introduction to Fourier Optics*, 3rd ed. (Roberts & Company, 2005).
- [24] A. E. Siegman, *Lasers* (University Science Books, 1986).
- [25] N. N. Lebedev, *Special Functions & Their Applications* (Dover, 1972).

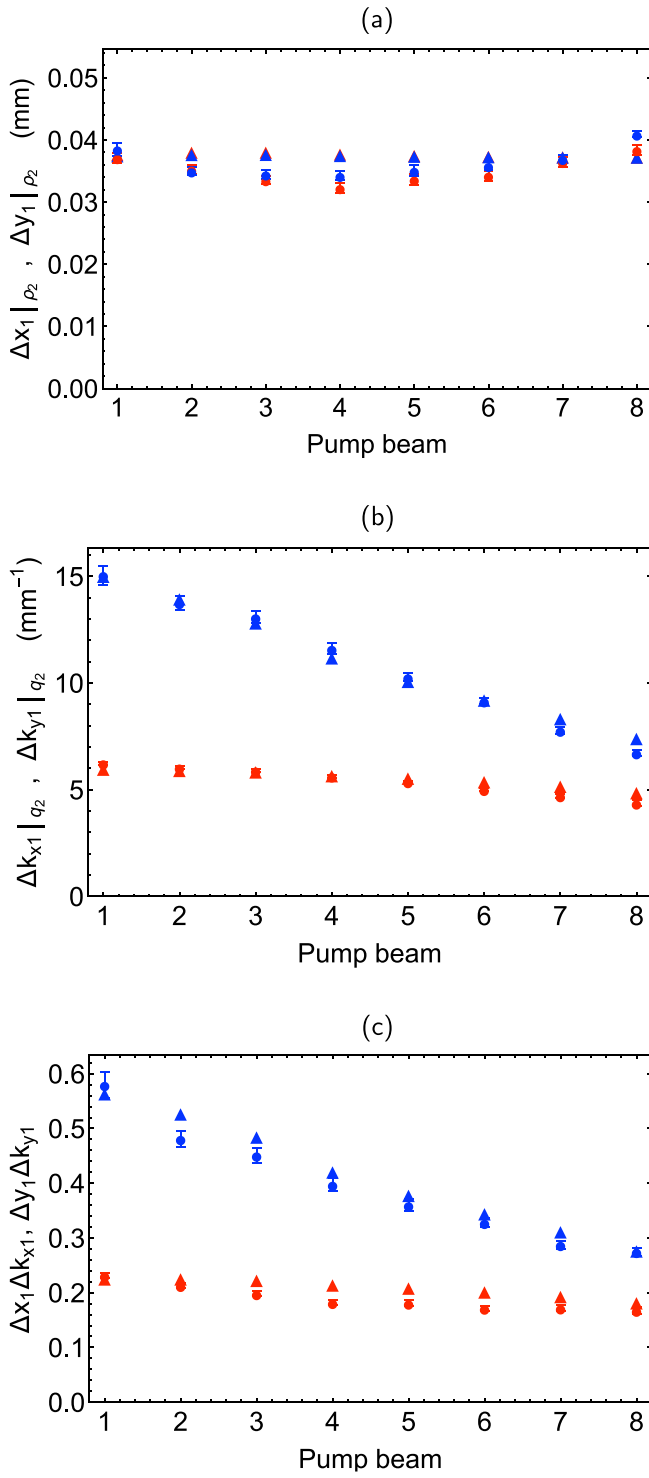


FIG. 7. Measured (\bullet) and predicted (\blacktriangle) values of (a) Δx_1 (red) and Δy_1 (blue), (b) Δk_{x1} (red) and Δk_{y1} (blue), (c) $\Delta x_1 \Delta k_{x1}$ (red) and $\Delta y_1 \Delta k_{y1}$ (blue) for a 5 mm-long BBO crystal pumped by 355 nm laser beams whose parameters are listed in Table I.